The BTK-DDX41 axis of the STING pathway is activated during cytomegalovirus lytic infection

Vargab Baruah[1] and Christine M. O'Connor[1,2,3]*

[1] Infection Biology; Sheikha Fatima bint Mubarak Global Center for Pathogen and Human Health Research, Lerner Research Institute, Cleveland Clinic, Cleveland, OH, 44195 USA; baruahv@ccf.org (V.B.); oconnoc6@ccf.org (C.M.O'C.)
[2] Case Comprehensive Cancer Center, Cleveland, OH 44106 USA; oconnoc6@ccf.org (C.M.O'C.)
[3] Molecular Medicine, Cleveland Clinic Lerner College of Medicine of Case Western Reserve University, Cleveland Clinic, Cleveland, OH 44195 USA; oconnoc6@ccf.org (C.M.O'C.)
* Corresponding author: oconnoc6@ccf.org

Abstract

The innate immune response is the first line of defense against invading pathogens, including the betaherpesvirus, human cytomegalovirus (CMV). The host's innate response acts as the first line of defense, and CMV, like other viruses, has consequently evolved multiple mechanisms to manipulate host interferon (IFN) responses. DEAD-box Helicase 41 (DDX41) is an intracellular dsDNA sensor that, upon activation by Bruton's tyrosine kinase (BTK), triggers type I IFN production through the Stimulator of Interferon Genes (STING) signaling pathway. Here, we show the activation of this signaling pathway during lytic CMV infection, wherein BTK, DDX41, and STING are activated through tyrosine phosphorylation, and both DDX41 and BTK interact with STING. Further, CMV infection re-localizes DDX41 from the nucleus to the cytoplasm, where it localizes to the perinuclear virus assembly compartment (vAC). Here, DDX41 phosphorylation is attenuated, suggesting cytoplasmic redistribution leads to a less active or inactive form. Additionally, DDX41 co-localizes in the vAC with the CMV tegument proteins, pp65 and pp71, each of which interact with DDX41 in immunoprecipitation assays. We further demonstrate the protective role of this signaling pathway, as treatment with the BTK inhibitor, orelabrutinib, attenuates DDX41 phosphorylation/activation and supports increased expression of viral proteins and virus replication. In sum, our work highlights the important role of BTK-DDX41-STING signaling in the innate immune response against CMV, which the virus subverts by attenuating its cytoplasmic activity, thereby diverting it from its typically protective function.

Importance

Human cytomegalovirus (CMV) is a ubiquitous pathogen that poses a significant threat to immunocompromised individuals, highlighting the critical role of innate immunity in controlling this viral infection. Despite extensive research, the complex mechanisms underlying innate immunity against CMV and the virus's strategies for evading immune detection remain only partially understood. This study identifies the activation of the cellular BTK-DDX41-STING innate signaling axis during lytic CMV

infection, which ultimately results in protective interferon responses. Our findings show that CMV infection triggers the cytoplasmic redistribution of the cellular protein, DDX41, leading to reduced phosphorylation and activity, thereby undermining its protective function. Additionally, pharmacological inhibition of BTK enhances viral protein expression and replication, highlighting the importance of this pathway in immune defense. Our work identifies BTK- and DDX41-dependent STING signaling as important for innate immune responses against CMV and further advances our understanding of CMV's manipulation of these responses.

Keywords

CMV, DDX41, STING, BTK, cytomegalovirus

50 **Introduction**

51 Human cytomegalovirus (CMV), a widespread beta-herpesvirus, infects 40% to 60% of adults in
52 developed countries, with seropositivity nearing 100% in developing nations (1). Following primary CMV
53 infection, the virus enters a latent phase within myeloid cells, characterized by viral genome
54 maintenance and suppressed infectious virus production. Latent CMV can intermittently reactivate
55 under certain conditions of immune system dysfunction and cellular differentiation, resulting in the lytic
56 replication of infectious virus (2). While primary infection and reactivation events are typically
57 asymptomatic, they can be severe in immunocompromised, immunosuppressed, or immuno-naïve
58 individuals, potentially causing serious organ-specific diseases or even death. A substantial proportion
59 of the population, even in developed countries, is immunologically vulnerable. In the US, about 3% of
60 adults are immunocompromised, and 6.6% are immunosuppressed due to health conditions or their
61 treatments (3, 4). Among immuno-naïve neonates, approximately 1 in 200 babies has congenital CMV
62 infection (5), and up to 15% of these infants develop long-term sequelae (6). These data underscore
63 the need to more completely understand the viral and cellular factors that support CMV replication.

64 The severity and outcome of CMV infection largely depend on the early immune events, when
65 the host's innate immunity plays a crucial role (7). It can prevent the establishment of infection by
66 overwhelming CMV upon initial contact or confine the virus to the latent phase, preventing progression
67 to the lytic phase. Early immune responses often involve recognition of pathogen-associated molecular
68 patterns (PAMPs) – conserved molecular signatures found on pathogens - by the host's pattern
69 recognition receptors (PRRs), which heavily influence the subsequent immune strategy. CMV's double-
70 stranded DNA (dsDNA) genome is detected by dsDNA-sensing PRRs, triggering an immune signaling
71 cascade that results in the production of anti-viral interferons (IFNs) and interferon-stimulated genes
72 (ISGs) (8). Understanding these key immune responses at the molecular level is crucial, particularly in
73 the absence of a vaccine, to determine how CMV might subvert these mechanisms as it infects the
74 host.

75 Activation of key components of the innate immune response is intricately linked to the CMV life
76 cycle, with different viral components targeted based on their abundance and accessibility. CMV dsDNA
77 can bind cytosolic DNA receptors such as cyclic GMP-AMP synthase (cGAS) and interferon-γ inducible
78 protein 16 (IFI16). This DNA sensing is followed by activation of stimulator of interferon genes (STING;
79 also known as MITA and ERIS), a key mediator in subsequent downstream immune signaling. STING
80 activation leads to the recruitment and activation of TANK-binding kinase 1 (TBK1), which in turn
81 phosphorylates interferon regulatory factor 3 (IRF3). This activated IRF3 then translocates to the
82 nucleus, where it drives the expression of type I interferons (IFN) and other inflammatory cytokines,
83 thereby mounting a defense against the invading virus (9).

84 Host-driven immune responses against CMV are complex since CMV has evolved impressively
85 sophisticated methods of manipulating host factors. For instance, CMV's tegument protein pp65 and
86 late protein pUL31 bind cGAS, inhibiting its activity (10, 11). Additionally, the membrane protein pUL42
87 also binds cGAS, blocking both its DNA binding and its ability to oligomerize/activate (12). Similar
88 observations are reported for IFI16, where pp65 binds IFI16 and inhibits its DNA sensing by preventing
89 its aggregation and signal amplification (13, 14). CMV also modulates restriction factors downstream of
90 DNA sensing. The viral glycoprotein, US9, the tegument protein, pp71, and the latency-associated
91 protein, pUL138, each bind STING and impair immune signaling (15-17). In addition to directly inhibiting
92 immune signaling through binding, CMV also subverts the immune response by misdirecting the
93 localization of restriction factors. For instance, while nuclear IFI16 binds CMV DNA early in infection,
94 during later stages, it is phosphorylated by pUL97 and mis-localized to the cytoplasmic vAC (18). While
95 these studies highlight the intricate and diverse mechanisms the host employs against CMV, as well as
96 those the virus uses to counter them, our understanding of the array of innate immune sensors triggered
97 by CMV is likely incomplete.

98 DEAD-box helicase 41 (DDX41) is a helicase with a conserved Asp-Glu-Ala-Asp (DEAD) motif
99 that functions as a DNA sensor (19). Similar to other DNA sensors, such as cGAS and IFI16, DDX41
100 activity is regulated by tyrosine phosphorylation. Lee at al. demonstrated that Bruton's tyrosine kinase
101 (BTK) phosphorylates DDX41 enhancing its binding to adenovirus dsDNA and STING (20). Additionally,
102 herpes simplex virus type 1 (HSV-1) infection results in upregulation of DDX41, upon which it interacts
103 with cGAS, activates the STING signaling pathway, and promotes inflammatory cytokine production
104 (19). However, the role of the BTK-DDX41-STING signaling axis in CMV infection remains unknown.
105 Given that DDX41 shares many downstream effectors with cGAS and IFI16, and that CMV has a dsDNA
106 genome, we posited that this signaling pathway could function as part of the innate immune response
107 against CMV.

108 Here, we show that the BTK-DDX41-STING signaling axis is activated during lytic CMV
109 infection, involving tyrosine phosphorylation of the restriction factors, and interaction of STING with
110 DDX41 and BTK. Following infection, DDX41 re-localizes from the nucleus to the cytoplasm, where it
111 co-localizes with the tegument protein, pp65, in the perinuclear vAC. Additionally, cytoplasmic-localized
112 DDX41 displays reduced phosphorylation, indicating that its cytoplasmic redistribution leads to a less
113 active form of the protein. Finally, we demonstrate that inhibiting BTK with orelabrutinib reduces
114 phosphorylation and activation of BTK and DDX41, which increases viral protein expression and
115 replication. Our work reveals an important role of the BTK-DDX41-STING pathway in the innate immune
116 response to CMV and demonstrates a mechanism by which the virus disrupts this response.
117

118 **Materials and Methods**

119 *Cells and Viruses*

120 Primary newborn human foreskin fibroblasts (NuFF-1, passage 13-28; GlobalStem, Rockville, MD,
121 USA) were cultured in Dulbecco's modified Eagle medium (DMEM) with 10% fetal bovine serum (FBS),
122 2 mM L-glutamine, 0.1 mM non-essential amino acids, 10 mM HEPES, and 100 U/ml each of penicillin
123 and streptomycin. The cells were maintained at 37°C with 5% CO_2.

124 The bacterial artificial chromosome (BAC)-derived viruses, TB40/E*mCherry* (WT) (21) and
125 TB40/E*mCherry*-UL99eGFP (UL99*gfp*) (22, 23) were previously characterized. Virus stocks were
126 prepared as previously described (24). In brief, p0 stocks were generated by transfecting BAC DNA into
127 naïve NuFF-1 cells. When 100% cytopathic effect (CPE) was observed, p1 stocks were expanded on
128 naïve NuFF-1 cells and harvested when 100% CPE was observed. Virus was purified through a 20%
129 sorbitol (VWR) cushion, resuspended 1:1 in XVIVO-15 (Lonza) and 3% bovine serum albumin (BSA),
130 aliquoted, flash frozen in liquid nitrogen, and stored at -80°C. Virus stocks were titered on naïve NuFF-
131 1 cells by 50% tissue culture infectious dose ($TCID_{50}$) assay.

132 Cells were infected at the multiplicity of infection (MOI) and for the duration indicated in the text. Cells
133 were infected in DMEM containing viral inoculum for 1 h at 37°C, with gentle agitation every 15 minutes
134 (min). The cells were washed twice with 1X phosphate-buffered saline (PBS) and replenished with fresh
135 DMEM at 37°C.

136 *Protein, RNA, and DNA Analyses*

137 For protein analyses, cells were treated and harvested at the times indicated in the text and/or Figure
138 Legends. Where indicated, cells were transfected with 10 µg/ml of either poly(dA:dT) interferon
139 stimulatory DNA (ISD), or control ISD using Lipofectamine 2000. In all cases, cells were lysed on ice
140 for 1 hour (h) using radioimmunoprecipitation assay (RIPA) buffer (1.0% NP-40; 1.0% sodium
141 deoxycholate; 0.1% SDS; 0.15 M NaCl; 0.01 M NaPO4, pH 7.2; 2 mM EDTA), with vortexing every 15
142 min. For protein isolation in nuclear/cytoplasmic fractions, cell pellets were resuspended in lysis buffer
143 (10 mM HEPES, pH 7.5; 5 mM MgCl2; 15 mM KCl; 1 mM PMSF) and subjected to three freeze-thaw
144 cycles in liquid nitrogen. The resulting suspension was passed through a 27G needle 15 times. The
145 lysed cells were layered over 50% sucrose (w/v) and centrifuged; the supernatant collected as the
146 cytoplasmic fraction. The pellet containing nuclei was resuspended in lysis buffer and sonicated three
147 times. After centrifugation, the supernatant was collected as the nuclear fraction. In all cases, protein
148 concentrations were measured by Bradford assay with Protein Assay Dye Reagent Concentrate (Bio-
149 Rad). Samples were denatured at 95°C for 10 min. Equal protein concentrations of the samples were

150 separated by SDS-PAGE and transferred to 0.45 µm nitrocellulose membranes (Amersham) using a
151 semi-dry transfer method. The following antibodies were used at the specified concentrations: anti-BTK
152 (Cell Signaling Technology [CST], 1:5,000), anti-STING (CST, 1:5,000; MilliporeSigma, 1:5,000), anti-
153 p-STING (CST, 1:1000), anti-DDX41 (CST, 1:5,000), anti-TBK (CST, 1:5,000), anti-p-TBK (CST,
154 1:1000), anti-CMV IE1 (clone 1B12, 1:100, (25)), anti-CMV UL44 (Virusys, 1:2500), anti-CMV pp65
155 (clone 8A8, 1:50 (26)), anti-CMV pp71, anti-tubulin (MilliporeSigma, 1:5000), anti-H3 (Abcam, 1:5000),
156 anti-beta-actin-peroxidase (MilliporeSigma, 1:10,000), goat-anti-mouse horseradish peroxidase (HRP)
157 secondary and goat-anti-rabbit horseradish peroxidase (HRP) secondary (both from Jackson
158 ImmunoResearch Labs, 1:10,000). Relative protein levels were quantified by densitometry using
159 ImageJ (27).

160 To quantify transcripts, total RNA was isolated and purified using the High Pure RNA Isolation kit
161 (Roche) in accordance to the manufacturer's protocol. Equal RNA concentrations (1.0 µg) were then
162 used to generate cDNA with random hexamer primers and SYBR™ Green I Reagents (ThermoFisher
163 Scientific), and equal volumes of cDNA were used for quantitative polymerase chain reaction (qPCR).
164 The following primers were used for transcript quantification: *IFNB*, forward – 5'-
165 CTTGGATTCCTACAAAGAAGCAGC-3' and reverse – 5'- TCCTCCTTCTGGAACTGCTGCA -3';
166 *UL123*, forward – 5'-GCCTTCCCTAAGACCACCAAT-3' and reverse – 5'-
167 ATTTTCTGGGCATAAGCCATAATC-3'; *GAPDH*, forward – 5'-CTGTTGCTGTAGCCAAATTCGT-3'
168 and reverse – 5'-ACCCACTCCTCCACCTTTGAC-3'. Samples were analyzed in triplicate using a 96-
169 well-format CFX Connect Real Time PCR machine (Bio-Rad), and expresion quantified relative to host
170 *GAPDH* expression.

171 To quantify CMV genomic DNA, NuFF-1 fibroblasts were infected (MOI = 0.5 $TCID_{50}$/cell) with WT virus.
172 At each indicated time point, cells were harvested and samples were treated with RNaseA (100 µg/mL)
173 for 1 h at 37°C to remove RNA. DNA was isolated by phenol-chloroform-isoamyl alcohol extraction,
174 followed by ethanol precipitation and resuspension in 10 mM Tris-HCl, pH 8.0 with 0.1 mM EDTA. Equal
175 sample volume was quantified by qPCR using the following primers: viral UL69, forward – 5'-
176 GGCTGATGATCTTGCGGGAA-3' and reverse – 5'-CGAGAGTCTACGTCTGGCAC-3'; cellular MDM2,
177 forward – 5'-CCCCTTCCATCACATTGCA-3' and reverse – 5'-AGTTTGGCTTTCTCAGAGATTTCC-3'.
178 UL69 and MDM2 abundance was quantified against a viral BAC standard (TB40/E-BACstandard),
179 which contains an MDM2 gene fragment (28). All samples were analyzed in triplicate, then normalized
180 to cellular MDM2.

181

182 *Immunofluorescence Assays*

183 Cells were cultured on coverslips in 6-well tissue culture plates (3×10^5 cells per well) and infected (MOI
184 = 0.5 $TCID_{50}$/cell) as described above. After 96 hpi, cells were washed three times with 1X PBS, fixed
185 with 2% paraformaldehyde for 15 min at 37°C, and then permeabilized with 0.1% Triton X-100 for 15
186 min at room temperature. The cells were washed three times with 0.25% (w/v) saponin and
187 subsequently blocked with 1X PBS containing 10% (v/v) human serum (Sigma Aldrich) and 0.25% (w/v)
188 saponin. Cells were incubated with primary antibodies against STING, BTK, phospho-BTK-Y551 (all
189 from Cell Signaling Technology, 1:1000), DDX41 (Cell Signaling Technology, 1:1,000), and STING
190 (MilliporeSigma, 1:1,000) in 10% (v/v) human serum and 0.25% (w/v) saponin for 1 h at room
191 temperature. Following this, the cells were washed three times with 0.25% (w/v) saponin and incubated
192 with Alexa-488-conjugated anti-mouse and Alexa-647-conjugated anti-rabbit secondary antibodies
193 (both from Thermo Fisher, 1:1,000) for 1 h at room temperature, shielded from light. Finally, coverslips
194 were mounted with FluorSave reagent (MilliporeSigma) onto slides and visualized using a Leica SP8
195 inverted confocal microscope with a 63x oil immersion objective. Colocalization in immunofluorescent
196 images was quantified using Volocity software. To assess colocalization of DDX41 or TBK1 with STING,
197 we calculated the percentage of mCherry-positive, CMV-infected cells that exhibited overlap between
198 the Volocity-defined compartments of each protein and STING. Quantification was performed on three
199 fields of view per condition, and the resulting percentages were plotted as bar graphs.

200 *Co-immunoprecipitation*

201 Cells were lysed in 1.0 ml of immunoprecipitation (IP) buffer [25 mM Tris, pH 7.4; 1 mM $MgCl_2$; 2 mM
202 EDTA; 1.0% Triton-X 100; 150 mM NaCl; Complete Protease Inhibitor Cocktail (Roche)] on ice for 2 h.
203 Protein G beads (100 µl; Protein G-sepharose Fast Flow, MilliporeSigma) were washed twice with IP
204 buffer (500 x *g*, 5 min), blocked for 1 h in 5.0% BSA in IP buffer, and then resuspended in 1.0 ml IP
205 buffer. The samples were clarified by centrifugation (12,000 x *g*, 10 min, 4°C), and 50 µl of the sample
206 (10%) was retained as the "input" control. The remaining sample was divided into two aliquots, each
207 incubated overnight at 4°C with protein G beads and either 2 µg of the specific precipitating antibody
208 or an isotype-matched IgG control antibody. The next day, the samples were centrifuged at 500 x *g* for
209 5 min, and 50 µl was reserved as the "unbound" sample. The samples were then washed four times
210 with IP wash buffer [25 mM Tris, pH 7.4; 10 mM $MgCl_2$; 2 mM EDTA; 0.1% Triton-X 100], with 50 µL
211 retained after washes 1 and 4. After the final wash, proteins in all samples were denatured using 2X
212 SDS and heating at 95°C for 10 min. The samples were then separated by SDS-PAGE and transferred
213 to nitrocellulose as described above.

214 *Toxicity Assay*

215 NuFF-1 cells (1.75 x 10^4 cells/well) were plated onto 96-well opaque white CulturPlate (Perkin
216 Elmer) and allowed to adhere overnight. Cells were then treated with orelabrutinib (GLPBio) in nine two-
217 fold dilutions (0.078 to 20 μM) for 24 h, followed by three washes with 1X PBS. Cell viability was
218 assessed after 2 and 5 days (i.e., 3 and 6 days post-treatment) using CellTiter-Glo (Promega) according
219 to the manufacturer's guidelines, and the plates were read with a Cytation 5 (Agilent) plate reader.
220 DMSO (equivalent v/v) served as the diluent and vehicle control, while puromycin (ranging from 20 μM
221 to 0.08 μM) was used as a positive control.

222 *Quantification of viral lytic replication*

223 NuFF-1 cells were treated with 0.5 μM orelabrutinib (GLPBio) prior to infection with TB40/E*mCherry*
224 (MOI = 0.01 $TCID_{50}$/cell) for 1 h, with gentle agitation every 15 min. After adsorption, cells were washed
225 three times with 1X PBS, and fresh media (V_f = 2.0 ml) containing 0.5 μM Orelabrutinib was added.
226 Cell-free virus (350 μl) was collected over a 16 day (d) timecourse, and 250 μl of fresh media with 100
227 μl of 10 μM orelabrutinib was added to restore the total volume to 2 ml. DMSO (equivalent v/v) served
228 as the diluent and vehicle control. Cell-associated virus was harvested at the final time point (16 days
229 post-infection; dpi) by lysing the cells through three freeze-thaw cycles. The clarified supernatant was
230 then used to determine the cell-assocated viral titer. Cell-free and cell-associated virus were quantified
231 by $TCID_{50}$ assay on naïve NuFF-1 fibroblasts.

232

233 **Results**

234 *BTK-DDX41-STING signaling is activated during lytic CMV infection*

235 Emerging data reveal an antiviral role for DDX41 (19, 29-31), though whether DDX41 functions as a
236 restriction factor during CMV infection remains unclear. To begin to address this, we first assessed the
237 expression and activation of restriction factors associated with the BTK-DDX41-STING signaling
238 pathway during lytic CMV replication. We mock- or lytically-infected NuFF-1 fibroblasts with
239 TB40/E*mCherry* (wild type; WT) over a 96 hour (h) time course, after which we measured protein BTK,
240 STING, DDX41 and TBK1 abundance and phosphorylation, which is essential for activation of these
241 restriction factors (20, 32-34). Additionally, we probed for the viral protein, IE1. As a control for BTK and
242 DDX41 activation, we transfected parallel cultures with poly(dA:dT) (29). Since there is no phospho-
243 specific antibody for DDX41, and the phospho-BTK antibody is ineffective in immunoblot assays, we
244 performed immunoprecipitation with a pan-phospho-tyrosine antibody, followed by immunoblot using
245 antibodies directed at total forms of either BTK or DDX41. Our data indicate BTK is activated by 6 h
246 post-infection (hpi), which is increased through 96 hpi (**Fig. 1A**). Similarly, DDX41 is also activated at 6

247 hpi, with sustained increased phosphorylation through the 96 h time point. Additionally, total DDX41 is
248 also increased over the time course, relative to mock-infected cultures (**Fig. 1B**). Levels of both total
249 and phosphorylated forms of BTK and DDX41 were comparable to those induced by poly(dA:dT)
250 transfection over a similar time course, although poly(dA:dT) transfection triggered an earlier and more
251 rapidly peaked response (**Fig. 1A, 1B**). We also observed an increase in phospho-forms of STING and
252 TBK1 to levels consistent with their activation following interferon stimulatory DNA (ISD) transfection
253 (**Fig. 1C**), which is a positive control for STING-TBK1 activation (35). Finally, we quantified mRNA
254 expression of *IFNB*, which encodes IFN-β, a protein upregulated in response to innate immune signals.
255 Infection induces a time-dependent increase in *IFNB* transcription, which peaks at 3 hpi and is sustained
256 throughout the time course (**Fig. 1D**). We consistently observed increased activation of BTK and DDX41
257 at 96 hpi, with sustained activation of STING and TBK1 through this time point. Overall, these data
258 indicate CMV induces both the abundance and phosphorylated activation of BTK, DDX41, STING, and
259 TBK1, which results in increased *IFNB* expression in infected fibroblasts.

260 To investigate the signaling mechanism and confirm pathway activation, we used
261 immunofluorescence assays (IFA) to examine colocalization and co-immunoprecipitation (co-IP) to
262 assess interactions among restriction factors, with a particular focus on STING. Previous studies have
263 shown STING physically interacts with many of its signaling partners, such as TBK1 and IRF3, bringing
264 them into close proximity for phosphorylation and subsequent activation (36). We mock- or WT-infected
265 NuFF-1 fibroblasts for 96 h and visualized colocalization of each restriction factor (BTK, pBTK-Y551,
266 DDX41 and TBK) with STING by immunoflourescence. We found BTK (**Fig. 2A**), its activated form
267 pBTK-Y551 (**Fig. 2B**), DDX41 (**Fig. 2C**), and TBK1 (**Fig. 2D**) each colocalize with STING at the
268 perinuclear region of the infected cell. We quantified the colocalization of STING with upstream DDX41
269 and downstream TBK1 in infected cells expressing mCherry between 24 and 96 hpi and found
270 consistent colocalization during this period in approximately 40–50% of cells (**Fig. 2C, 2D**).
271 Quantification in mCherry-positive cells was not possible between 3-12 hpi due to the absence of
272 mCherry expression (**Fig. S1**). Further, we confirmed the interaction between STING and BTK (**Figs.
273 3A, S2A**), as well as STING and DDX41 (**Figs. 3B, S2B**) by co-IP, consistent with previous findings
274 (20, 37). We also confirmed CMV infection by IE1 protein abundance (**Fig. S2C,D**). Collectively, our
275 data reveal BTK-DDX41-STING signaling is activated following WT infection,.

276

277 *CMV redistributes a fraction of DDX41 to the cytoplasm*

278 Our data reveal CMV infection results in distinct changes in the subcellular localization of the restriction
279 factors, including DDX41 (**Fig. 2**). In the absence of infection (mock control), DDX41 primarily displays

280 nuclear localization; however, CMV infection results in the progressive migration of this host restriction
281 factor to the perinuclear region as early as 24 hpi. DDX41 cytoplasmic localization increases as infection
282 progresses and is observed in about 50-60% of all infected cells at 72 and 96 hpi (**Fig. 2C**). This is
283 consistent with previous work revealing DNA stimulation triggers DDX41 relocalization (19). Further,
284 the CMV-induced perinuclear relocalization of DDX41 suggested to us that this host protein may
285 become co-localized within the CMV vAC. To test this, we infected fibroblasts with a recombinant virus,
286 TB40/E*mCherry*-UL99*gfp*, which contains eGFP fused to the carboxy terminus of the *UL99* ORF (22,
287 23). *UL99* encodes pp28, a viral protein that localizes to the vAC during lytic infection (38), which we
288 also confirmed (**Fig. 4A**). Similar to our data in **Fig. 2C**, we noted a portion of DDX41 relocalizes to the
289 vAC (**Fig. 4A**). Additionally, the other DDX41-associated restriction factors (BTK, STING, TBK1) also
290 relocalize to the vAC following CMV lytic infection (**Fig. S3**).To gain a better understanding of the
291 abundance of DDX41 that was relocalized in response to CMV infection, we analyzed protein lysates
292 derived from nuclear and cytoplasmic fractions of mock- or WT-infected cells over a time course of
293 infection. In mock-infected cells, DDX41 retains its nuclear localization. However, in CMV-infected
294 fibroblasts, a portion of DDX41 is translocated to the cytoplasm as early as 24 hpi, which increases and
295 persists through the time course we evaluated (**Fig. 4B**). We confirmed this cytoplasmic shuttling of
296 DDX41 to the perinuclear vAC between 24 and 96 hpi by IFA for DDX41 and pp65, a viral protein that
297 also localizes to the vAC during lytic infection (**Figs. 4C, S4**). We hypothesized that since DDX41 is a
298 dsDNA sensor, perhaps a portion of DDX41 is retained within the nucleus by the host cell to target the
299 viral genome. To test this, we evaluated whether DDX41 colocalizes with the CMV DNA polymerase
300 subunit, UL44, which we used to identify sites of viral genome replication by IFA. Although a fraction
301 of DDX41 remains in the nucleus during infection, nuclear DDX41 does not specifically colocalize with
302 UL44 (**Fig. 4D**). Taken together, our data indicate DDX41 is relocalized from the nucleus to perinuclear,
303 cytoplasmic regions consistent with the vAC in the majority of infected cells late times in infection.

304 In addition to relocalizing this antiviral protein, we hypothesized that CMV infection may also
305 result in altered activity of the cytoplasmic portion of DDX41. Thus, we next asked whether perinuclear-
306 localized DDX41 exhibited altered signaling potency compared to its nuclear counterpart. To this end,
307 we analyzed the tyrosine phosphorylation of DDX41 in nuclear and cytoplasmic fractions of cells that
308 were either mock- or WT-infected, first confirming the fractionation using tubulin and H3 as cytoplasmic
309 and nuclear loading controls, respectively (**Fig. 5A**). We then performed immunoprecipitation with a
310 phospho-tyrosine antibody and probed for DDX41 in these fractions. Under mock conditions, DDX41 is
311 localized to the nucleus, consistent with our findings above, where it is phosphorylated. During infection,
312 although total DDX41 is more abundant in the cytoplasm than in the nucleus, the
313 phosphorylated/activated fraction in the cytoplasm is greatly reduced, as indicated by a reduction in the

314 p-Tyr DDX41 pulldown from the cytoplasmic fraction (**Fig. 5B**). Taken together, these data indicate
315 CMV infection induces a relocalization of a fraction of the inactivated form of DDX41 to the cytoplasm.

316

317 *DDX41 interacts with CMV-encoded tegument proteins*

318 Previous reports have noted a similar CMV-induced perinuclear distribution of the dsDNA sensor, IFI16.
319 At later stages of infection, IFI16 is localized to the vAC, where it interacts with the tegument protein,
320 pp65, to collectively subvert IFI16-mediated DNA sensing (10, 13, 18). Indeed, pp65 also interacts with
321 cGAS, thereby interfering with cGAS-STING interaction and innate sensing activity (10). In parallel,
322 *UL82*-encoded tegument protein, pp71, interacts with host restriction factors, ultimately preventing the
323 proper assembly of the STING-TBK1-IRF complex, whose activity is required for innate sensing via this
324 pathway (39). Based on these observations, as well as our IFAs showing colocalization of DDX41 and
325 pp65 between 24 and 96 hpi (**Fig. 4C**), we hypothesized that a similar interaction between CMV-
326 encoded tegument proteins and DDX41 regulates this host restriction factor's localization and activity
327 following CMV infection. To this end, we infected fibroblasts and assessed the potential co-localization
328 and interaction between DDX41 and either pp65 or pp71. Our findings reveal DDX41 co-localizes with
329 pp65 (**Fig. 6A**) and pp71 (**Fig. 6B**) in the perinuclear vAC. Further, DDX41 interacts with pp65 (**Fig. 6C**)
330 as well pp71, though detection of this latter interaction is far weaker than the former (**Fig. 6D**). These
331 results suggest that pp65, and to a lesser extent, pp71, interact with DDX41, likely retaining this host
332 restriction factor in the cytoplasmic vAC.

333

334 *Activated BTK-DDX41-dependent STING signaling limits CMV protein expression and replication*

335 Since our data indicate BTK, DDX41, and STING are activated upon lytic CMV infection, we next
336 assessed the impact of this branch of STING signaling on infection. To this end, we utilized
337 pharmacological inhibition using orelabrutinib, a highly specific and irreversible BTK inhibitor (40). Since
338 BTK activates DDX41 (20), we posited this would serve as a reasonable approach to inhibit DDX41, as
339 our attempts of both knockout and knockdown of this protein were unsuccessful (data not shown). This
340 is perhaps not surprising, as DDX41 is embryonic lethal (30, 41). Using the pharmacological approach
341 instead, we first evaluated the toxicity and efficacy of orelabrutinib in our model system and observed
342 minimal toxicity over a concentration range of 0.078 to 20 μM. To validate the assay, we included
343 puromycin treatment as a positive control (**Fig. S6A**). We also evaluated the impact of orelabrutinib
344 treatment on the signaling pathway using a multipronged approach. We assessed DDX41 protein
345 abundance following orelabrutinib treatment at various concentrations (0.1–10 μM) and durations (24–

346 120 h at 0.5 μM). DDX41 abundance was attenuated following 0.5 μM orelabrutinib treatment, which
347 was further decreased with increasing concentration of orelabrutinib (**Fig. S6B**) and longer treatment
348 times (**Fig. S6C**). Additionally, orelabrutinib treatment reduced *IFNB* transcription in WT-infected cells,
349 although this reduction was not statistically significant (**Fig. S6D**). Despite this, we did observe
350 diminished phosphorylation of BTK (**Fig. S7A**) and DDX41 (**Fig. S7B**) in orelabrutinib-treated, WT-
351 infected cells compared to untreated counterpart cultures in IP-western assays (**Fig. S7**) . Our data also
352 reveal orelabrutinib-treated, WT-infected cells display a reduction in total DDX41 abundance (**Fig. S7B**),
353 which likely also contributes to attenuated phosphorylation levels of this protein. Collectively, these data
354 suggest that orelabrutinib inhibit BTK and DDX41 activity without causing toxicity in fibroblasts.

355 Having an effective means by which to target BTK-DDX41, we leveraged orelabrutinib to assess
356 the impact of inhibiting BTK-DDX41-dependent STING signaling on lytic CMV infection. To this end, to
357 determine the impact of orelabrutinib-mediated DDX41 inhibition on viral protein translation, we
358 evaluated the abundance of representative viral proteins from the early and late kinetic classes.
359 Orelabrutinib-treated, WT-infected cells displayed a reduction in the expression of BTK, DDX41, and
360 STING compared to infected cells treated with DMSO (- orelabrutinib; **Fig 7A**). Concurrent with the
361 reduced abundance of these restriction factors, we observed increased abundance of the viral early
362 protein, UL44, and the viral late protein, pp65 (**Fig. 7A**). In parallel, we evaluated CMV genome copy
363 number in WT-infected fibroblasts treated with 0.5 μM orelabrutinib or DMSO (- orelabrutinib) over a 96
364 h time course. We find a statistically significant increase of viral genomes at 72 hpi in orelabrutinib-
365 treated cells (**Fig. 7B**). We also evaluated multistep viral growth over a 16-day time course, which
366 revealed orelabrutinib treatment resulted in an increase in cell-free virus production from 8 – 16 dpi,
367 with a statistically significant increase at 12 dpi (**Fig. 7C**). Additionally, cell-associated virus also
368 increased in the presence of orelabrutinib, although not to statistically significant levels (**Fig. 7D**). In
369 sum, these data show that attenuation of BTK-DDX41-dependent signaling promotes CMV lytic
370 replication, indicating a role for this branch of STING signaling during CMV infection.

371

372 **Discussion**

373 Here we show BTK-DDX41-dependent STING signaling functions in the innate immune response
374 against lytic CMV infection. Specifically, our data reveal this branch of STING signaling is activated
375 through the interaction of BTK and DDX41 with STING (**Figs. 1-3)**. Further, CMV infection induces a
376 cytoplasmic redistribution of DDX41 and its associated restriction factors to the perinuclear vAC (**Fig.**
377 **4**), where it exhibits reduced activation, as evidenced by decreased tyrosine phosphorylation (**Fig. 5**)
378 and interacts with the CMV tegument proteins pp65 and pp71 (**Fig. 6**). Additionally, we demonstrate

379 the protective nature of this signaling pathways by pharmacological inhibition of BTK using orelabrutinib,
380 an inhibitor that attenuates this signaling axis and results in increased viral protein abundance and CMV
381 replication (**Fig. 7**). Collectively, our findings underscore the significance of this signaling pathway and
382 reveal a mechanism by which CMV evades the immune response (**Fig. 8**).

383 dsDNA sensors are of considerable interest in the context of CMV, as several, including cGAS,
384 IFI16, AIM2, and ZBP1, trigger IFN production upon detection of the CMV genome (42-45). Our findings
385 herein now add DDX41 to this growing repertoire of sensors that are involved in the innate response
386 against CMV. Our study shows that lytic CMV infection induces the abundance of BTK, DDX41, STING,
387 and TBK1, as well as accumulation of *IFNB* transcripts. We confirmed the activation of the pathway, as
388 evidenced by the phosphorylation of BTK, DDX41 and STING, with both BTK and DDX41 colocalizing
389 and interacting with STING. Previous research showed DDX41 interacts with STING at its second to
390 fourth transmembrane domains in poly(dA)-stimulated myeloid dendritic cells (29). Additionally, in a
391 HEK293T-based overexpression system, the BTK SH3/SH2-interaction domain binds the
392 transmembrane region of STING (20). This mediatory role of STING is well-documented; for example,
393 STING interacts with TBK1 and IRF3, and then facilitates the phosphorylation and activation of IRF3 by
394 TBK1 (36). We hypothesize a similar mechanism based on the results from our study - after BTK and
395 DDX41 bind STING, BTK could activate DDX41 through phosphorylation. Although it remains unclear
396 whether STING directly induces this phosphorylation or merely facilitates the proximity of BTK and
397 DDX41, current data suggest STING likely plays a more active role in the process.

398 Multiple studies have highlighted CMV's diverse mechanisms to counteract DNA sensor-
399 dependent immunity at various levels. At the DNA sensing level, CMV UL31 interacts with cGAS,
400 causing the dissociation of DNA from cGAS and negatively regulating the STING signaling pathway
401 (11). Similarly, UL42 binds cGAS, in turn inhibiting its DNA binding, oligomerization, and enzymatic
402 activity (12). The tegument protein, pp65, also binds cGAS, preventing its interaction with STING and
403 thus inactivating STING signaling (10). pp65 also interacts with IFI16's PYRIN domain, blocking its
404 oligomerization upon DNA sensing and subsequent immune signaling (14). Here, we observed the
405 formation of the nascent vAC using pp65 beginning at 24 hpi - the same time point at which DDX41
406 was detected in the cytoplasmic fraction. This observation, as well as the documented propensity of
407 viral proteins, particularly pp65, to bind dsDNA sensors, drew our attention to tegument proteins and
408 their potential interaction with DDX41. Indeed, we found DDX41 associates with both pp65 and, to a
409 lesser extent, pp71 during lytic CMV infection. The decreased detection of pp71 does not necessarily
410 imply a weaker or less probable interaction, but rather could result from diminished availability of pp71
411 for interaction with DDX41 compared to pp65.

412 What remains outstanding is whether the interaction between DDX41 and pp65 and/or pp71 is
413 required for relocalizing DDX41 to the vAC or whether these interactions serve to keep DDX41 in the
414 vAC once DDX41 is already there. While possible, it is unlikely the tegument proteins aid in DDX41
415 redistribution. Others have reported DDX41 relocalization to perinuclear regions in response to DNA
416 stimuli (19, 46), which Singh and colleagues demonstrated is dependent upon acetylation of DDX41's
417 most amino-terminal nuclear localization signal (NLS; (19)). It is thus likely that DDX41 cytoplasmic
418 localization during CMV infection is stimulated in a similar fashion, dependent upon DNA sensing, as
419 opposed to specific, CMV-encoded factors. Why would CMV-encoded tegument proteins interact with
420 vAC-localized DDX41? It is possible the tegument proteins interact with DDX41 to retain this host
421 protein in a less active state late in infection. We showed cytoplasmic DDX41 activity is attenuated,
422 despite its colocalization with STING and BTK in the perinuclear region. It is attractive to hypothesize
423 that the interaction with the tegument proteins precludes DDX41 activation, similar to what is reported
424 for cGAS and IFI16 (10, 14). Alternatively, perhaps the CMV tegument protein(s)-DDX41 interaction
425 results in DDX41's incorporation into the mature viral particle, similar to that reported for IFI16 (18). This
426 could ensure DDX41 is delivered to newly infected cells, allowing for its immediate action for very early
427 innate responses following infection. This latter hypothesis could support the basis for the more late-
428 phase phenotypes we observed herein. Further, virion-delivered DDX41 may indicate additional
429 functions beyond innate immune responses, similar to IFI16, which also interacts with pp65 to activate
430 viral gene transcription at the major immediate early promoter (14). DDX41 may have additional
431 functions during CMV infection, as this host protein additionally coordinates RNA splicing and
432 transcriptional elongation, thereby preventing DNA replication stress (47). Thus, one could posit
433 DDX41's functions during CMV infection are more extensive, raising the possibility its potential inclusion
434 in the virion serves a biologically important purpose. These are compelling questions warranting further
435 exploration, and experiments to address these possibilities are on-going.

436 Our findings herein highlight the protective role of BTK-DDX41-dependent STING signaling in
437 the immune response to CMV lytic infection and further reveals a mechanism of immune evasion
438 through disrupted activation and localization of DDX41. Our work advances our understanding of innate
439 responses against CMV, providing insights that could inform strategies to counteract CMV's immune
440 evasive strategies.

441

442 **Acknowledgements**
443 The authors thank Ian Groves for helpful discussions and Ganes Sen for critical reading of the
444 manuscript. The authors also thank Amanda Mendelsohn (Cleveland Clinic Enterprise Creative
445 Services) for assistance with the graphical image.

Funding

This work was supported in part by the National Institutes of Health Core Instrument award (S10OD019972; awarded to Judy Drazba, Director, Cleveland Clinic Imaging Core).

References

1. Griffiths P, Reeves M. 2021. Pathogenesis of human cytomegalovirus in the immunocompromised host. Nat Rev Microbiol 19:759-773.
2. Smith NA, Chan GC, O'Connor CM. 2021. Modulation of host cell signaling during cytomegalovirus latency and reactivation. Virol J 18:207.
3. Antinori A, Bausch-Jurken M. 2023. The Burden of COVID-19 in the Immunocompromised Patient: Implications for Vaccination and Needs for the Future. J Infect Dis 228:S4-S12.
4. Martinson ML, Lapham J. 2024. Prevalence of Immunosuppression Among US Adults. JAMA 331:880-882.
5. Jones CE, Bailey H, Bamford A, Calvert A, Dorey RB, Drysdale SB, Khalil A, Heath PT, Lyall H, Ralph KMI, Sapuan S, Vandrevala T, Walter S, Whittaker E, Wood S, Collaboration UKCCI. 2023. Managing challenges in congenital CMV: current thinking. Arch Dis Child 108:601-607.
6. Boppana SB, Ross SA, Fowler KB. 2013. Congenital cytomegalovirus infection: clinical outcome. Clin Infect Dis 57 Suppl 4:S178-81.
7. Dell'Oste V, Biolatti M, Galitska G, Griffante G, Gugliesi F, Pasquero S, Zingoni A, Cerboni C, De Andrea M. 2020. Tuning the Orchestra: HCMV vs. Innate Immunity. Front Microbiol 11:661.
8. Marques M, Ferreira AR, Ribeiro D. 2018. The Interplay between Human Cytomegalovirus and Pathogen Recognition Receptor Signaling. Viruses 10.
9. Almine JF, O'Hare CA, Dunphy G, Haga IR, Naik RJ, Atrih A, Connolly DJ, Taylor J, Kelsall IR, Bowie AG, Beard PM, Unterholzner L. 2017. IFI16 and cGAS cooperate in the activation of STING during DNA sensing in human keratinocytes. Nat Commun 8:14392.
10. Biolatti M, Dell'Oste V, Pautasso S, Gugliesi F, von Einem J, Krapp C, Jakobsen MR, Borgogna C, Gariglio M, De Andrea M, Landolfo S. 2018. Human Cytomegalovirus Tegument Protein pp65 (pUL83) Dampens Type I Interferon Production by Inactivating the DNA Sensor cGAS without Affecting STING. J Virol 92.
11. Huang ZF, Zou HM, Liao BW, Zhang HY, Yang Y, Fu YZ, Wang SY, Luo MH, Wang YY. 2018. Human Cytomegalovirus Protein UL31 Inhibits DNA Sensing of cGAS to Mediate Immune Evasion. Cell Host Microbe 24:69-80 e4.
12. Fu YZ, Guo Y, Zou HM, Su S, Wang SY, Yang Q, Luo MH, Wang YY. 2019. Human cytomegalovirus protein UL42 antagonizes cGAS/MITA-mediated innate antiviral response. PLoS Pathog 15:e1007691.
13. Cristea IM, Moorman NJ, Terhune SS, Cuevas CD, O'Keefe ES, Rout MP, Chait BT, Shenk T. 2010. Human cytomegalovirus pUL83 stimulates activity of the viral immediate-early promoter through its interaction with the cellular IFI16 protein. J Virol 84:7803-14.
14. Li T, Chen J, Cristea IM. 2013. Human cytomegalovirus tegument protein pUL83 inhibits IFI16-mediated DNA sensing for immune evasion. Cell Host Microbe 14:591-9.
15. Choi HJ, Park A, Kang S, Lee E, Lee TA, Ra EA, Lee J, Lee S, Park B. 2018. Human cytomegalovirus-encoded US9 targets MAVS and STING signaling to evade type I interferon immune responses. Nat Commun 9:125.
16. Nukui M, Roche KL, Jia J, Fox PL, Murphy EA. 2020. Protein S-Nitrosylation of Human Cytomegalovirus pp71 Inhibits Its Ability To Limit STING Antiviral Responses. J Virol 94.
17. Albright ER, Mickelson CK, Kalejta RF. 2021. Human Cytomegalovirus UL138 Protein Inhibits the STING Pathway and Reduces Interferon Beta mRNA Accumulation during Lytic and Latent Infections. mBio 12:e0226721.
18. Dell'Oste V, Gatti D, Gugliesi F, De Andrea M, Bawadekar M, Lo Cigno I, Biolatti M, Vallino M, Marschall M, Gariglio M, Landolfo S. 2014. Innate nuclear sensor IFI16 translocates into the cytoplasm during the early stage of in vitro human cytomegalovirus infection and is entrapped in the egressing virions during the late stage. J Virol 88:6970-82.

498 19. Singh RS, Vidhyasagar V, Yang S, Arna AB, Yadav M, Aggarwal A, Aguilera AN, Shinriki S,
499 Bhanumathy KK, Pandey K, Xu A, Rapin N, Bosch M, DeCoteau J, Xiang J, Vizeacoumar FJ, Zhou Y,
500 Misra V, Matsui H, Ross SR, Wu Y. 2022. DDX41 is required for cGAS-STING activation against DNA
501 virus infection. Cell Rep 39:110856.
502 20. Lee KG, Kim SS, Kui L, Voon DC, Mauduit M, Bist P, Bi X, Pereira NA, Liu C, Sukumaran B, Renia L,
503 Ito Y, Lam KP. 2015. Bruton's tyrosine kinase phosphorylates DDX41 and activates its binding of
504 dsDNA and STING to initiate type 1 interferon response. Cell Rep 10:1055-65.
505 21. O'Connor CM, Shenk T. 2011. Human cytomegalovirus pUS27 G protein-coupled receptor homologue
506 is required for efficient spread by the extracellular route but not for direct cell-to-cell spread. J Virol
507 85:3700-7.
508 22. Nukui M, O'Connor CM, Murphy EA. 2018. The Natural Flavonoid Compound Deguelin Inhibits HCMV
509 Lytic Replication within Fibroblasts. Viruses 10.
510 23. O'Connor CM, Nukui M, Gurova KV, Murphy EA. 2016. Inhibition of the FACT Complex Reduces
511 Transcription from the Human Cytomegalovirus Major Immediate Early Promoter in Models of Lytic and
512 Latent Replication. J Virol 90:4249-4253.
513 24. O'Connor CM, Shenk T. 2012. Human cytomegalovirus pUL78 G protein-coupled receptor homologue is
514 required for timely cell entry in epithelial cells but not fibroblasts. J Virol 86:11425-33.
515 25. Zhu H, Shen Y, Shenk T. 1995. Human cytomegalovirus IE1 and IE2 proteins block apoptosis. J Virol
516 69:7960-70.
517 26. Bechtel JT, Shenk T. 2002. Human cytomegalovirus UL47 tegument protein functions after entry and
518 before immediate-early gene expression. J Virol 76:1043-50.
519 27. Schneider CA, Rasband WS, Eliceiri KW. 2012. NIH Image to ImageJ: 25 years of image analysis. Nat
520 Methods 9:671-5.
521 28. Krishna BA, Wass AB, O'Connor CM. 2020. Activator protein-1 transactivation of the major immediate
522 early locus is a determinant of cytomegalovirus reactivation from latency. Proc Natl Acad Sci U S A
523 117:20860-20867.
524 29. Zhang Z, Yuan B, Bao M, Lu N, Kim T, Liu YJ. 2011. The helicase DDX41 senses intracellular DNA
525 mediated by the adaptor STING in dendritic cells. Nat Immunol 12:959-65.
526 30. Stavrou S, Aguilera AN, Blouch K, Ross SR. 2018. DDX41 Recognizes RNA/DNA Retroviral Reverse
527 Transcripts and Is Critical for In Vivo Control of Murine Leukemia Virus Infection. mBio 9.
528 31. Duan Y, Zeng J, Fan S, Liao Y, Feng M, Wang L, Zhang Y, Li Q. 2019. Herpes Simplex Virus Type 1-
529 Encoded miR-H2-3p Manipulates Cytosolic DNA-Stimulated Antiviral Innate Immune Response by
530 Targeting DDX41. Viruses 11.
531 32. Rawlings DJ, Scharenberg AM, Park H, Wahl MI, Lin S, Kato RM, Fluckiger AC, Witte ON, Kinet JP.
532 1996. Activation of BTK by a phosphorylation mechanism initiated by SRC family kinases. Science
533 271:822-5.
534 33. Wang C, Wang X, Veleeparambil M, Kessler PM, Willard B, Chattopadhyay S, Sen GC. 2020. EGFR-
535 mediated tyrosine phosphorylation of STING determines its trafficking route and cellular innate immunity
536 functions. EMBO J 39:e104106.
537 34. Wang C, Sharma N, Veleeparambil M, Kessler PM, Willard B, Sen GC. 2021. STING-Mediated
538 Interferon Induction by Herpes Simplex Virus 1 Requires the Protein Tyrosine Kinase Syk. mBio
539 12:e0322821.
540 35. Zhang G, Chan B, Samarina N, Abere B, Weidner-Glunde M, Buch A, Pich A, Brinkmann MM, Schulz
541 TF. 2016. Cytoplasmic isoforms of Kaposi sarcoma herpesvirus LANA recruit and antagonize the innate
542 immune DNA sensor cGAS. Proc Natl Acad Sci U S A 113:E1034-43.
543 36. Tanaka Y, Chen ZJ. 2012. STING specifies IRF3 phosphorylation by TBK1 in the cytosolic DNA
544 signaling pathway. Sci Signal 5:ra20.
545 37. Parvatiyar K, Zhang Z, Teles RM, Ouyang S, Jiang Y, Iyer SS, Zaver SA, Schenk M, Zeng S, Zhong W,
546 Liu ZJ, Modlin RL, Liu YJ, Cheng G. 2012. The helicase DDX41 recognizes the bacterial secondary
547 messengers cyclic di-GMP and cyclic di-AMP to activate a type I interferon immune response. Nat
548 Immunol 13:1155-61.
549 38. Sanchez V, Sztul E, Britt WJ. 2000. Human cytomegalovirus pp28 (UL99) localizes to a cytoplasmic
550 compartment which overlaps the endoplasmic reticulum-golgi-intermediate compartment. J Virol
551 74:3842-51.
552 39. Fu YZ, Su S, Gao YQ, Wang PP, Huang ZF, Hu MM, Luo WW, Li S, Luo MH, Wang YY, Shu HB. 2017.
553 Human Cytomegalovirus Tegument Protein UL82 Inhibits STING-Mediated Signaling to Evade Antiviral
554 Immunity. Cell Host Microbe 21:231-243.
555 40. Dhillon S. 2021. Orelabrutinib: First Approval. Drugs 81:503-507.

41. Stepanchick E, Wilson A, Sulentic AM, Choi K, Hueneman K, Starczynowski DT, Chlon TM. 2024. DDX41 haploinsufficiency causes inefficient hematopoiesis under stress and cooperates with p53 mutations to cause hematologic malignancy. Leukemia 38:1787-1798.
42. Paijo J, Doring M, Spanier J, Grabski E, Nooruzzaman M, Schmidt T, Witte G, Messerle M, Hornung V, Kaever V, Kalinke U. 2016. cGAS Senses Human Cytomegalovirus and Induces Type I Interferon Responses in Human Monocyte-Derived Cells. PLoS Pathog 12:e1005546.
43. Gariano GR, Dell'Oste V, Bronzini M, Gatti D, Luganini A, De Andrea M, Gribaudo G, Gariglio M, Landolfo S. 2012. The intracellular DNA sensor IFI16 gene acts as restriction factor for human cytomegalovirus replication. PLoS Pathog 8:e1002498.
44. Huang Y, Ma D, Huang H, Lu Y, Liao Y, Liu L, Liu X, Fang F. 2017. Interaction between HCMV pUL83 and human AIM2 disrupts the activation of the AIM2 inflammasome. Virol J 14:34.
45. DeFilippis VR, Alvarado D, Sali T, Rothenburg S, Fruh K. 2010. Human cytomegalovirus induces the interferon response via the DNA sensor ZBP1. J Virol 84:585-98.
46. Ma JX, Li JY, Fan DD, Feng W, Lin AF, Xiang LX, Shao JZ. 2018. Identification of DEAD-Box RNA Helicase DDX41 as a Trafficking Protein That Involves in Multiple Innate Immune Signaling Pathways in a Zebrafish Model. Front Immunol 9:1327.
47. Shinriki S, Hirayama M, Nagamachi A, Yokoyama A, Kawamura T, Kanai A, Kawai H, Iwakiri J, Liu R, Maeshiro M, Tungalag S, Tasaki M, Ueda M, Tomizawa K, Kataoka N, Ideue T, Suzuki Y, Asai K, Tani T, Inaba T, Matsui H. 2022. DDX41 coordinates RNA splicing and transcriptional elongation to prevent DNA replication stress in hematopoietic cells. Leukemia 36:2605-2620.

Figure Legends

Figure 1. CMV infection induces a time-dependent increase in BTK, DDX41, STING, TBK1 abundance and activation, as well as *IFNB* mRNA expression. (**A, B**) NuFF-1 fibroblasts were mock- or WT-infected (MOI = 0.5 $TCID_{50}$/cell) or transfected with 10 µg/mL poly(dA:dT). At the indicated times post-infection or -transfection, cells were immunoprecipitated (IP) with antibodies specific for phosphorylated-tyrosine (p-Tyr) or IgG. Immunoprecipitates were then probed for BTK and DDX41 by western blot (WB). Input for the IPs are also shown. N = 3; representative blots shown. (**C**) NuFF-1 fibroblasts were mock- or WT-infected (MOI = 0.5 $TCID_{50}$/cell) or transfected with 10 µg/mL interferon stimulatory DNA (ISD) or ISD control DNA. At the indicated times post-infection or -transfection, cells were collected and equal concentration (30 µg) of lysates were probed for phosphorylated (p) and total forms of the cellular proteins, STING and TBK1, as well as the viral protein, IE1. Cellular β-actin was probed as a loading control. N = 3, representative blots shown. (**E**) Total RNA was isolated at the indicated times post-infection, and *IFNB* was measured by RT-qPCR and plotted in arbitrary units (AU) as ΔΔCt relative to cellular *GAPDH*. N = 3 biological replicates, each with technical triplicates; representative experiment shown.

Figure 2. BTK, DDX41, and TBK1 co-localize with STING during CMV infection. NuFF-1 fibroblasts were mock- or WT-infected (MOI = 0.5 $TCID_{50}$/cell), after which cells were processed for immunofluorescence assay (IFA) at (**A, B**) 96 hpi or (**C,D**) over a time course of infection. The early time points (3-12 hpi) for the data in (**C,D**) are shown in Fig. S1. Cells were then probed with antibodies directed at: (**A**) BTK, (**B**) pBTK-Y551, (**C**) DDX41, or (**D**) TBK1 (each shown in white), as well as (**A-D**) STING (green). (**C,D**; inset graph) The percentage of infected, mCherry-positive cells displaying (**C**) STING and DDX41 or (**D**) STING and TBK1 colocalization was quantified using Volocity. mCherry (red) is a marker of lytic infection; nuclei were visualized with DAPI (blue). Inset in the WT merge panel is enlarged at right. Images were acquired using 63x objective. N = 3; representative images shown.

Figure 3. BTK and DDX41 interact with STING during CMV infection. NuFF-1 fibroblasts were mock- or WT-infected (MOI = 0.5 $TCID_{50}$/cell) for the indicated times. Cells were then harvested, and immunoprecipitated (IP) with antibodies specific for (**A**) BTK, (**B**) DDX41, or (**A,B**) IgG.

Immunoprecipitates were then probed for STING by western blot (WB). I, input; U, unbound; 1, wash #1; 4, wash #4; P, IP sample. N = 3; representative blots shown.

Figure 4. DDX41 is translocated from the nucleus to the perinuclear viral assembly compartment (vAC). (**A**) NuFF-1 fibroblasts were mock- or *UL99gfp*-infected (MOI = 0.5 $TCID_{50}$/cell) for 96 h. Cells were then fixed, permeabilized, and stained for DDX41 (white). mCherry (red) is a marker of lytic infection, pp28-eGFP is shown in green, and nuclei were visualized with DAPI (blue). vAC, viral assembly compartment. (**B**) NuFF-1 fibroblasts were mock- or WT-infected (MOI = 0.5 $TCID_{50}$/cell) for the indicated times. Lysates (20 µg) from nuclear (N) and cytoplasmic (C) fractions were probed for DDX41, tubulin (cytoplasmic marker), and histone H3 (nuclear marker). N = 3; representative blots shown. (**C, D**) NuFF-1 fibroblasts were infected as in (**B**). (**C**) At the indicated times post-infection or (**D**) 96 hpi, cells were fixed, permeabilized, and stained for (**C**) pp65 or (**D**) pUL44 (each shown in green) and DDX41 (white). mCherry (red) is a marker of lytic replication and DAPI (blue) was used to visualize nuclei. Viral replication compartment (RC) is indicated. (**A,C,D**). Inset in the merge panel is enlarged at right. Images were acquired using 63x objective. N = 3; representative images shown.

Figure 5. Cytoplasmic DDX41 exhibits attenuated phosphorylation. NuFF-1 fibroblasts were mock- or WT-infected (MOI = 0.5 $TCID_{50}$/cell). At 96 hpi, cells were harvested and nuclear (N) and cytoplasmic (C) fractions isolated. (**A**) Nuclear (N) and cytoplasmic (C) fractions were probed for tubulin (cytoplasmic), histone H3 (nuclear), or DDX41. (**B**) Fractions from (**A**) were then immunoprecipitated (IP) with antibodies specific phosphorylated Tyrosine (p-Tyr) or IgG and were then probed for DDX41 by western blot (WB). I, input; U, unbound; 1, wash #1; 4, wash #4; P, IP sample. N = 3; representative blots shown.

Figure 6. CMV tegument proteins, pp65 and pp71, interact with DDX41 and co-localize with DDX41 in the vAC. NuFF-1 fibroblasts were mock- or WT-infected (MOI = 0.5 $TCID_{50}$/cell) for 96 h. (**A,B**) Cells were fixed, permeabilized and stained for DDX41 (white) and either (**A**) pp65 (green) or (**B**) pp71 (green). (**A,B**) mCherry (red) is shown as a marker of infection, and nuclei were visualized with DAPI (blue). (**C,D**) Cells were then harvested, and proteins immunoprecipitated (IP) with antibodies specific for DDX41 or IgG. Immunoprecipitates were then probed for (**C**) pp65 or (**D**) pp71 by western blot (WB). Samples were also probed for DDX41 by western blot as a control (Fig. S5). (**C,D**) I, input; U, unbound; 1, wash #1; 4, wash #4; P, IP sample. N = 3; representative blots shown.

Figure 7. Orelabrutinib inhibition of BTK/DDX41 signaling induces lytic CMV infection. (**A, B**) NuFF-1 fibroblasts were pre-treated with 0.5 µM orelabrutinib (+ orelabrutinib) or DMSO (v/v; - orelabrutinib) for 1 h prior to mock or WT infection (MOI = 0.5 $TCID_{50}$/cell). (**A**) At 96 hpi, cells were harvested and lysates (25 µg) probed for the indicated proteins. N = 3; representative blots shown. (**B**) Cells were harvested and whole cell DNA was isolated at the indicated time-points. Viral and cellular DNA was quantified by qPCR using primers targeting the CMV UL69 non-promoter region and cellular MDM2, respectively. The ratio of UL69 to MDM2 is shown as arbitrary units (AU) and depicted as fold-change relative to the - orelabrutinib condition at 24 h. Data represent mean values from three biological replicates, each with three technical replicates. Error bars indicate SD of three biological replicates. Statistical significance was calculated using two-way ANOVA with Tukey's multiple comparisons test. Data are not significant unless otherwise noted; $^{*}p < 0.01$. (**C, D**) NuFF-1 fibroblasts were treated with 0.5 µM orelabrutinib (+ orelabrutinib; open triangles/dashed line) or DMSO (v/v; - orelabrutinib; open circles/solid line) for 1 h, and then infected with WT (MOI = 0.01 $TCID_{50}$/cell). Following adsorption, cells were washed and replenished with fresh media containing orelabrutinib (0.5 µM) or DMSO (v/v). (**C**) Cell-free virus was collected over a 16-day time course (- orelabrutinib, solid line; + orelabrutinib, dashed line), and (**D**) cell-associated virus was harvested at 16 dpi (- orelabrutinib, open bar; + orelabrutinib, checked bar). (**C,D**) Viral titers were quantified by $TCID_{50}$ using naïve NuFF-1 fibroblasts. Samples within a biological replicate were analyzed in triplicate. N = 3; representative experiment

660 shown. Data are mean±s.d. of the technical replicates (datapoints). Statistical significance was
661 calculated by paired t-test. Data are not significant unless otherwise noted; *$p < 0.05$.
662
663 **Figure 8. Model depicting displacement of host restriction factors during CMV lytic infection,**
664 **mitigating the protective DDX41/BTK/STING signaling axis.** BTK/DDX41/STING signaling is
665 protective against lytic CMV infection. Viral infection results in displacement of the restriction factors to
666 the virus assembly complex, where DDX41 interacts with CMV tegument proteins. Cytoplasmic
667 redistribution of these host factors results in their decreased activity that is otherwise important for
668 initiating antiviral signaling.

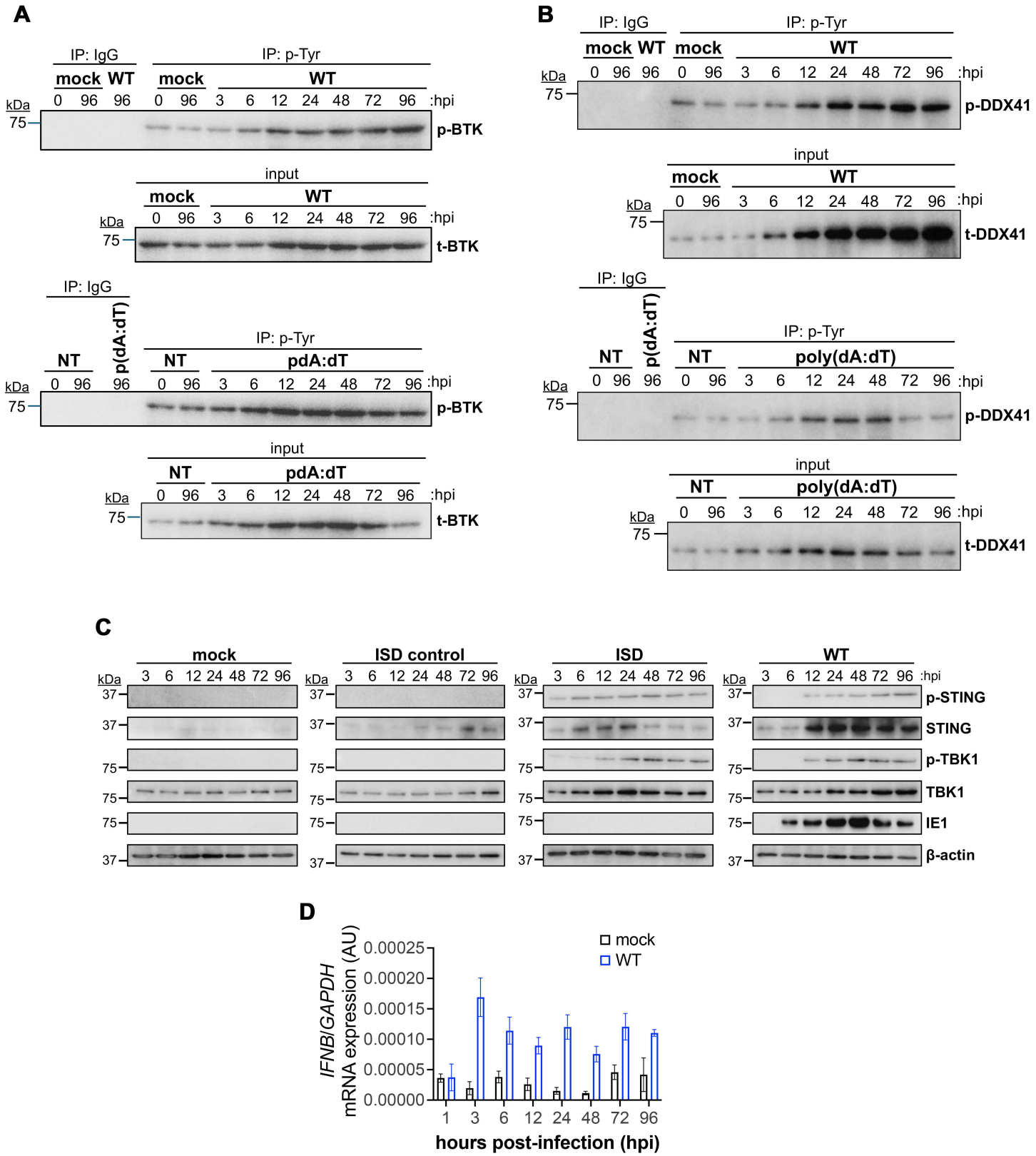
A
IP: IgG
IP: p-Tyr
mock WT
mock
WT
kDa
0 96 96 0 96 3 6 12 24 48 72 96 :hpi
75
p-BTK
input
mock
WT
0 96 3 6 12 24 48 72 96 :hpi
t-BTK
IP: IgG
p(dA:dT)
NT
IP: p-Tyr
NT
pdA:dT
p-BTK
input
NT
pdA:dT
t-BTK
B
IP: IgG
IP: p-Tyr
mock WT
mock
WT
p-DDX41
input
mock
WT
t-DDX41
IP: IgG
p(dA:dT)
NT
IP: p-Tyr
NT
poly(dA:dT)
p-DDX41
input
NT
poly(dA:dT)
t-DDX41
C
mock
ISD control
ISD
WT
3 6 12 24 48 72 96 :hpi
37
75
p-STING
STING
p-TBK1
TBK1
IE1
β-actin
D
IFNB/GAPDH
mRNA expression (AU)
0.00025
0.00020
0.00015
0.00010
0.00005
0.00000
mock
WT
1 3 6 12 24 48 72 96
hours post-infection (hpi)

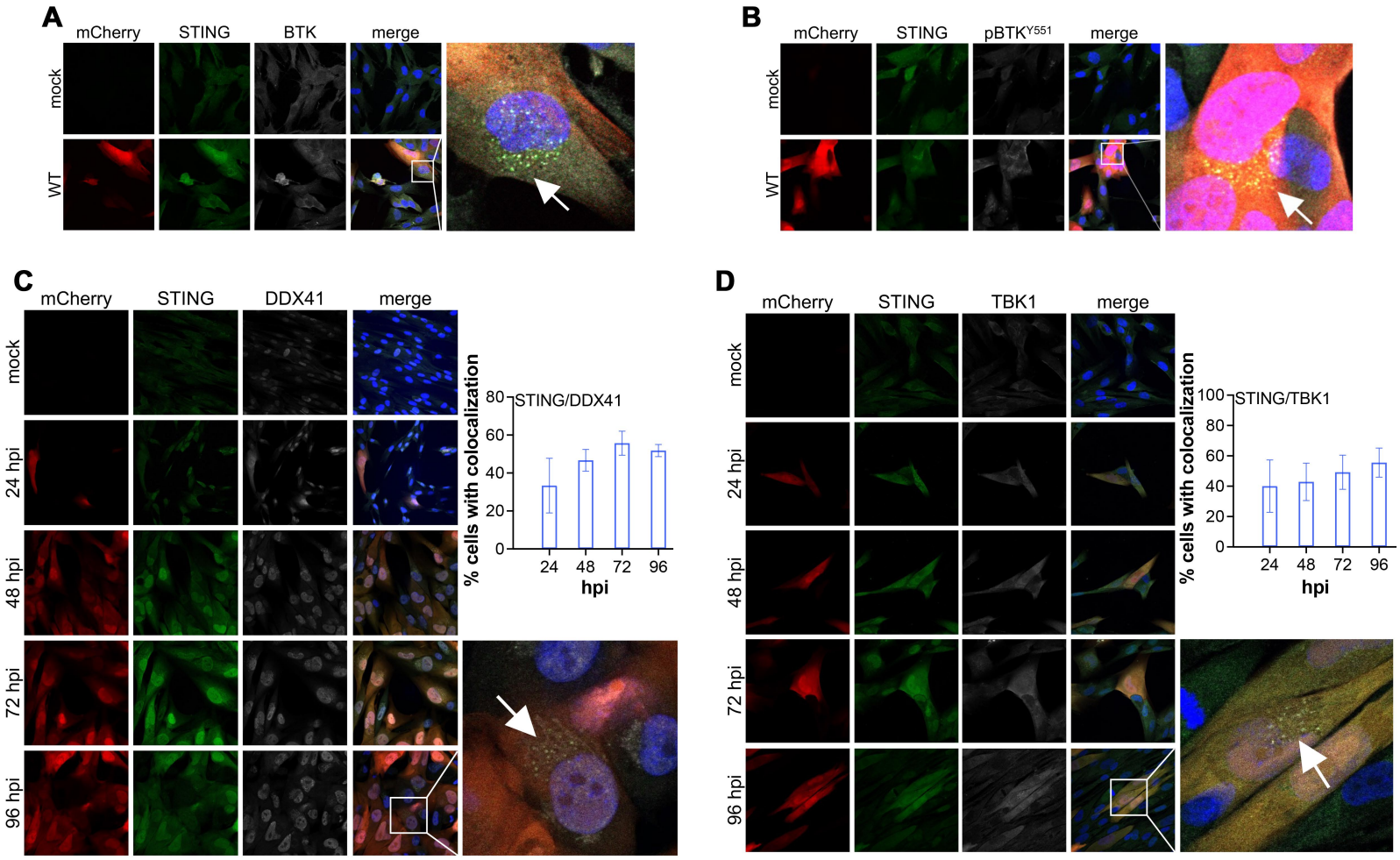
A
mCherry
STING
BTK
merge
mock
WT
B
mCherry
STING
pBTK^{Y551}
merge
mock
WT
C
mCherry
STING
DDX41
merge
mock
24 hpi
48 hpi
72 hpi
96 hpi
STING/DDX41
% cells with colocalization
0
20
40
60
80
24
48
72
96
hpi
D
mCherry
STING
TBK1
merge
mock
24 hpi
48 hpi
72 hpi
96 hpi
STING/TBK1
% cells with colocalization
0
20
40
60
80
100
24
48
72
96
hpi

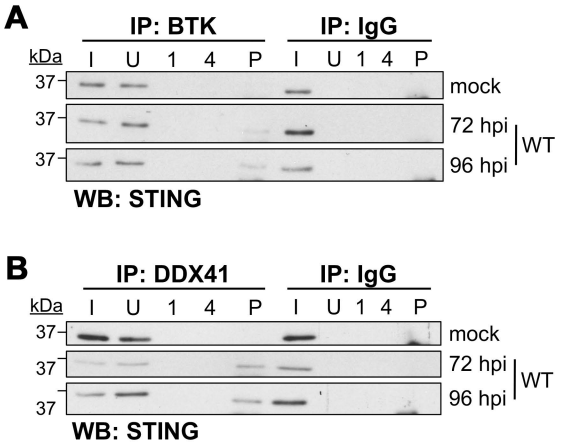
A
IP: BTK
IP: IgG
kDa
I U 1 4 P I U 1 4 P
37
37
37
mock
72 hpi
96 hpi
WT
WB: STING
B
IP: DDX41
IP: IgG
kDa
I U 1 4 P I U 1 4 P
37
37
37
mock
72 hpi
96 hpi
WT
WB: STING

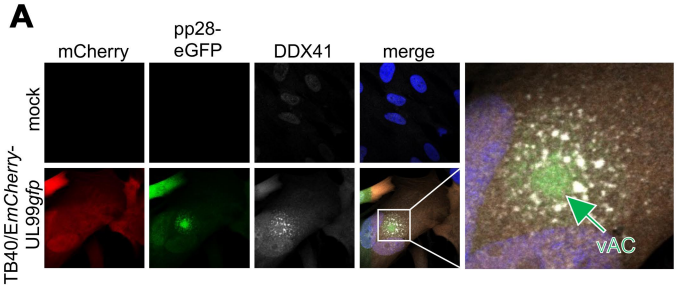
A
mCherry
pp28-eGFP
DDX41
merge
mock
TB40/EmCherry-UL99gfp
vAC

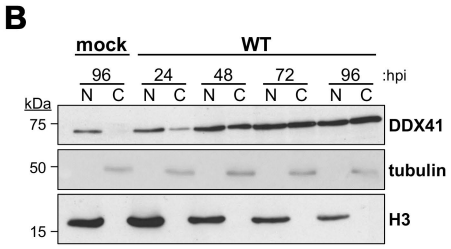
B
mock
WT
96
24
48
72
96
:hpi
N C N C N C N C N C
kDa
75
50
15
DDX41
tubulin
H3

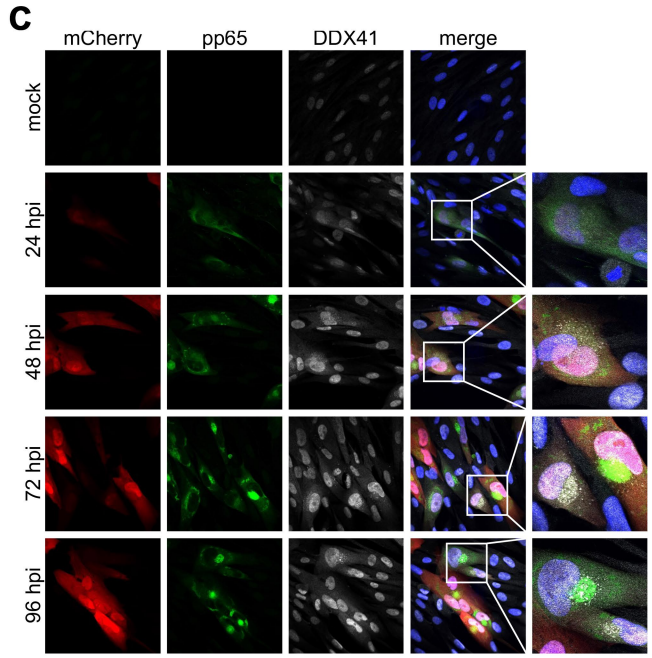
C
mCherry
pp65
DDX41
merge
mock
24 hpi
48 hpi
72 hpi
96 hpi

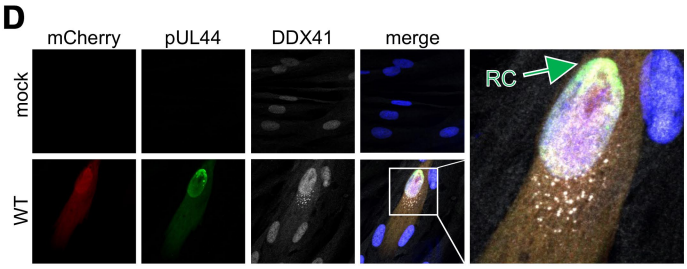
D
mCherry
pUL44
DDX41
merge
mock
WT
RC

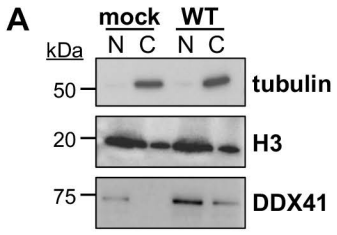
A
mock
WT
N C N C
kDa
50
tubulin
20
H3
75
DDX41

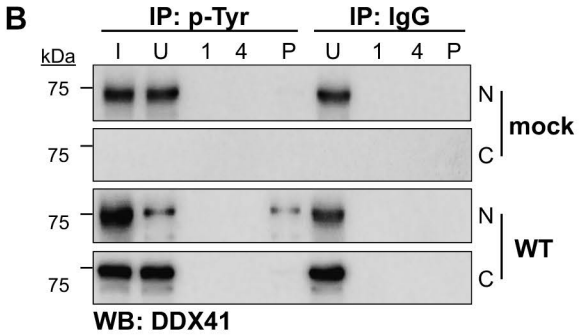
B
IP: p-Tyr
IP: IgG
kDa
I U 1 4 P U 1 4 P
75
N
mock
75
C
75
N
WT
75
C
WB: DDX41

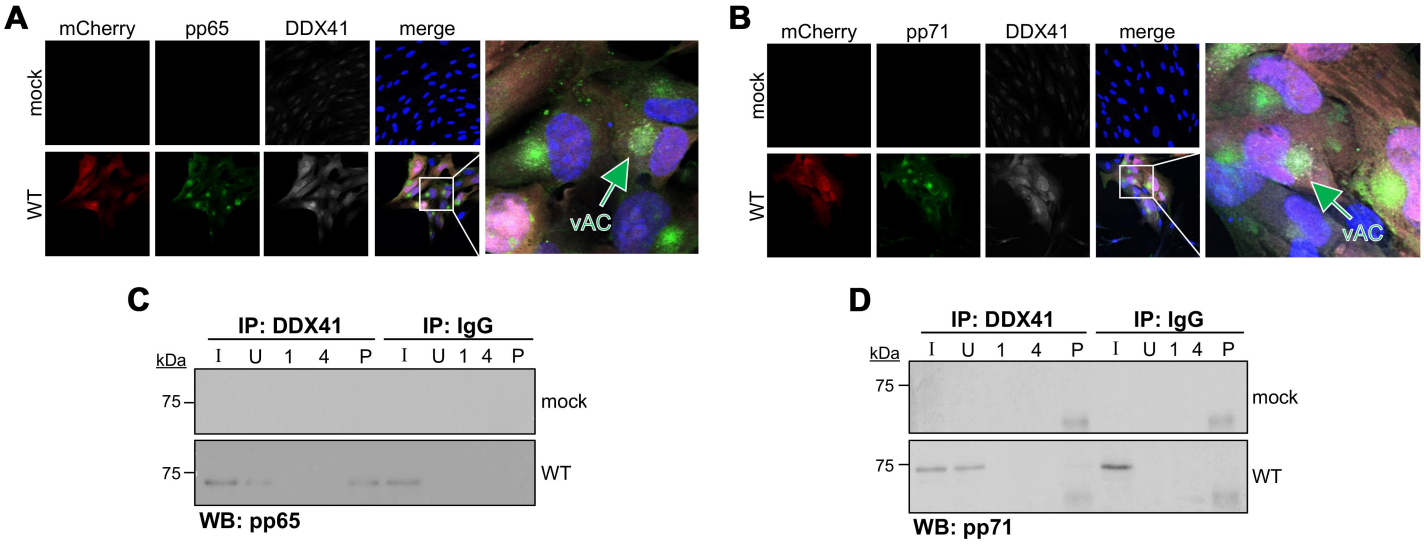
A
mCherry
pp65
DDX41
merge
mock
WT
vAC
B
mCherry
pp71
DDX41
merge
mock
WT
vAC
C
IP: DDX41
IP: IgG
kDa
I U 1 4 P I U 1 4 P
75
mock
75
WT
WB: pp65
D
IP: DDX41
IP: IgG
kDa
I U 1 4 P I U 1 4 P
75
mock
75
WT
WB: pp71

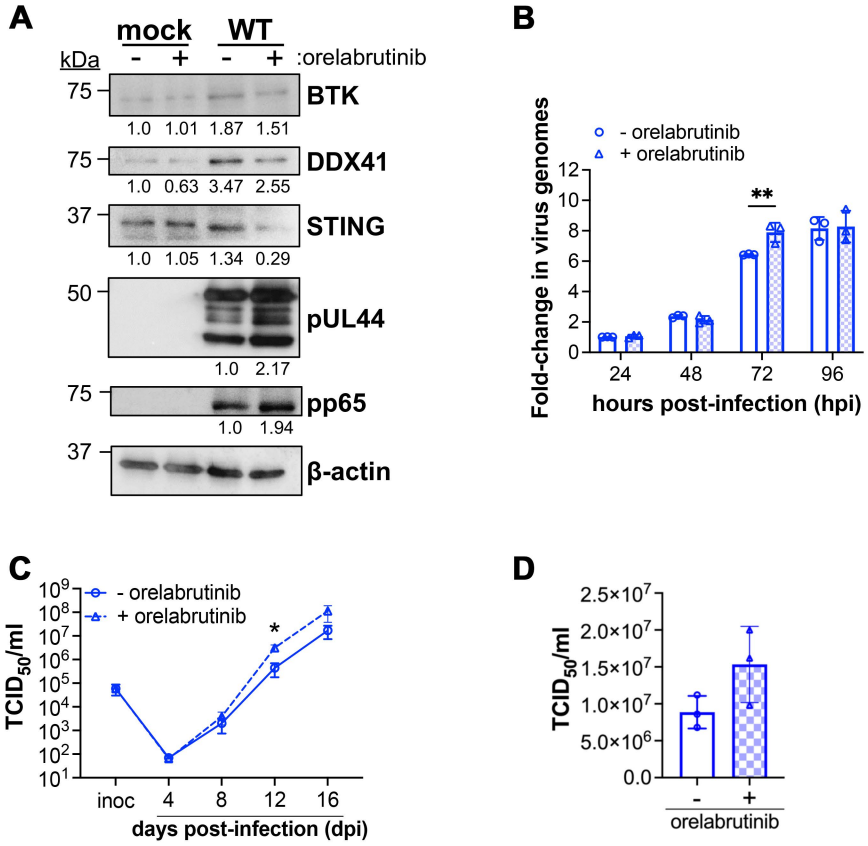
A
mock
WT
kDa
- + - + :orelabrutinib
75
BTK
1.0 1.01 1.87 1.51
75
DDX41
1.0 0.63 3.47 2.55
37
STING
1.0 1.05 1.34 0.29
50
pUL44
1.0 2.17
75
pp65
1.0 1.94
37
β-actin
B
- orelabrutinib
+ orelabrutinib
Fold-change in virus genomes
**
hours post-infection (hpi)
C
- orelabrutinib
+ orelabrutinib
TCID50/ml
*
inoc
days post-infection (dpi)
D
TCID50/ml
orelabrutinib

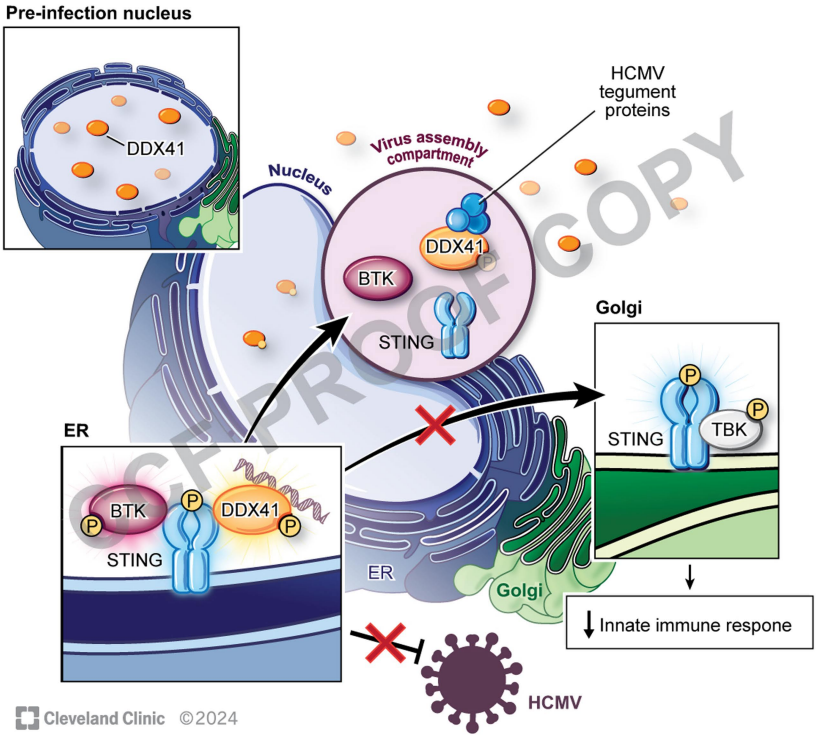

CCF PROOF COPY